The effect of magnesium doping concentration on the structural and optical properties of zinc oxide nanoparticles

M. S. Nazar[a], U. Mishal[b], M. Khalid[b], P. Fazil[c], M. Rahim[d,b,*]
[a]*Department of Physics Federal Urdu University of Arts, Science and technology Karach, Pakistan*
[b]*Department of Physics, University of Karachi, Pakistan*
[c]*Department of Chemistry, University of Karachi, Pakistan*
[d]*Department of Basic Sciences, DHA Suffa University, Karachi, Pakistan.*

In this study, the optical and structural properties of Magnesium doped Zinc Oxide ($Zn_{1-x}Mg_xO$) nanoparticles (x = 1%, 3%, and 5%) were examined. The synthesis was carried out at 300 ^oC by using a simple co-precipitation method. The structural samples were used to characterize the synthesized nanoparticles by using Scanning Electron Microscopy (SEM) and X-Ray Diffraction (XRD). Energy Dispersive X-Ray spectroscopy (EDX) was used to determine the chemical composition of the samples. Furthermore, UV-Vis spectroscopy was conducted to study our samples' optical characteristics. As per XRD analysis, both pure and Mg doped ZnO samples possess wurtzite structure. The particle size was revealed to decrease significantly with Mg concentration, from 36 nm for pure sample to 23.87 nm with 5% Mg. In comparison to ZnO, the XRD pattern of Mg-doped ZnO shows a peak shift towards lower 2θ values. As a result of deformation of crystal structure caused by integrated Mg^{+2} ions onto Zn^{+2} sites. SEM images of synthesized samples reveal that the nanoparticles possess sheet, spherical and rod like morphologies for different values of x. The EDX analysis verifies the purity of samples within the detection limits. According to optical absorption spectra obtained from UV-Visible spectroscopy in the 200nm to 1000nm range affirmed that as Mg concentration increased, the band gap increased from 3.37 eV for pure sample to 3.74 eV with 5% Mg. The UV-Visible spectra of pure ZnO and Mg-doped ZnO samples also exhibit distinct peaks in the UV region at 335 nm, 311 nm, 310.6 nm, and 310 nm. Across the spectra of pure and Mg-doped ZnO samples, the UV peak is attributed to free exciton transitions, whereas, in the spectra of Mg-doped ZnO UV absorbance peak in the visible region is attributed to the radiative transitions of electrons captured at oxygen vacant sites with holes trapped at singly ionized oxygen vacancies.

(Received February 21, 2022; Accepted July 29, 2022)

Keywords: Zinc oxide nanoparticles, Metallic nanoparticles, Magnesium doping, Effect of doping, Optical properties

1. Introduction

Zinc oxide is an intrinsic semiconductor material with vast range of applications including rubbers, glass, cement, plastics, ceramics, sealants, adhesives, lubricants, foods, paints, ointments, pigments, batteries, fire retardants, first-aid tapes, etc.[1] It belongs to II-VI semiconductor group and has wide energy band gap and high electron mobility.[2] Vacant oxygen positions in ZnO or the presence of zinc atoms in interstitial spaces typically result in n-type behavior.[3, 4]

Zinc oxide nanoparticles are extremely important because of their numerous uses, including chemical sensors, bio-sensors, gas sensors, cosmetics, drug delivery, and memory storage, window materials for displays, optical and electrical components, and solar cells.[5-7] ZnO is one of the basic materials for optoelectronic applications with short wavelengths due to its

* Corresponding author: muhammad.rahim@dsu.edu.pk
https://doi.org/10.15251/JOR.2022.184.565

high bond strength at room temperature, strong binding energy (60 meV) and wide band gap of 3.37 eV.[8] It is used in laser developments and blue to ultraviolet (UV) optoelectronics.[9, 10]

The crystal structure of zinc oxide is categorized into three types, i.e., cubic zincblende, cubic rocksalt and hexagonal wurtzite.[11] The wurtzite structure is the most stable and common among all forms of structures at ambient conditions.[12] The Zinc and Oxide centers in both types are tetrahedral, which is the most common geometry for Zn (II).[13] As high pressures of about 10 GPa are applied to a ZnO wurtzite or zincblende structure, it transforms to a rocksalt structure.[14] The zincblendes feature a cubic packing array of their atoms, while the wurtzites have a hexagonally packed lattice.[15]

The hexagonal structure's lattice constants are c = 5.2 and a = 3.25, making c/a ratio 1.60 approximately.[16] The bonding of ZnO is predominantly ionic (Zn^{+2} and O^{-2}), as it is in the majority of group II-VI compounds.[17] It also has strong piezoelectricity because of the polar Zinc and Oxygen bonds, while Zinc and Oxygen planes are electrically charged.[10, 18]

Lattice parameters are extremely important while assembling the semiconductor devices. The material's crystal lattice parameters can be determined using High Resolution X-Ray Diffraction (HRXRD). Many defects, however, disturb the lattice's strict periodicity. These defects can control the electrical, thermal, optical, and mechanical properties of semiconductors. Moreover, the lattice parameters govern the plasticity, hardness, thermal conductivity and electrical conductivity of semiconductors.[19-21]

1.1. Optical Properties of ZnO

The interaction with electromagnetic radiation within the visible region (with wavelengths ranging from 390 to 770 nm) is referred to as a material's optical property.[22] Planck's law describes the energy E of a photon as follows:

$$E = h\upsilon = \frac{hc}{\upsilon}$$

where, h is Plank's constant, υ is frequency of EM waves, c is speed of light in vacuum and λ *is* wavelength.[23, 24]

Semiconductors' optical properties are related to both intrinsic and extrinsic effects.[25] In UV to visible regions of the spectrum ZnO displays high efficiency for luminescence because of its wide band gap.[26] Based on its wide band gap competences, it has become an excellent material for both electronics and optoelectronics applications that include solar cells, gas sensors, heat mirrors and liquid crystal displays.[27, 28] Since ZnO has a very high exciton binding energy of 60 meV, excitonic transitions may occur at room temperature.[29] These transitions decrease the threshold voltage for laser emission while increasing the radiative recombination efficiency for spontaneous emission.[30] Various experimental techniques are available to analyze the optical transitions in ZnO, including optical propagation, optical reflection, optical reflectance, calorimetric spectroscopy, spectroscopic ellipsometry and photoluminescence (PL).[25, 31] Because of the existence of its green band, ZnO is regarded as a world's most trusted luminescent material and is used in planar displays and also in some screens with short-decay cathode luminescence.[32, 33]

1.2. Doping in ZnO

Doping is a commonly used technique for increasing the conductivity of semiconductors that involves introducing a very small amount of certain impurities into the pure semiconductor.[34] Since impurity atoms have a lower ionization energy than the host semiconductor's band-gap energy, they readily increase electrical conductivity.[35] In recent years, attention has been drawn to a multifunctional material (ZnO) with a promising direct band gap because of its excellent potential for short wavelength laser diodes in the UV spectrum, blue light emission instruments and detectors. It is currently acquiring popularity due to the large amount of engineering space available in its band gap and its ability of lasing in the UV region at room temperature.[32, 36-38]

ZnO is doped as both n-type and p-type semiconductor.[39] Unfortunately, doping p-type carriers in semiconductors with wide energy band gaps (such as GaN, ZnSe, ZnS, etc.) is a challenging process.[40] Although, unipolar doping of semiconductors having broad energy band gap is easily available, doping wide band gap semiconductors to n-type is easy but p-type doping is difficult.[41] Thus, zinc oxide is present in a variety of shapes of nanostructures, and each type of nanostructure exhibits a particular range of qualities like piezoelectricity, fine optical transparency, high electrical conductivity and prominent visible photoluminescence.[42, 43] These properties can be enhanced further by doping this extraordinary semiconductor material.[44]

2. Experimental Set Up

2.1. Materials

The materials used in this research work are Zinc Nitrate hexa hydrate, Zn (NO3)2. 6H2O of 99% purity (Merck), Magnesium Acetate, Mg (CH3COO) 2of 99% purity (Merck), Sodium Hydro Oxide (NaOH), Acetone, De-mineralized water. All of the materials we used in our research were of analytical grade.

2.2. Synthesis

The co-precipitation process is used to synthesize pure and Mg-doped zinc oxide because of its simplicity, cost effectiveness, and high efficiency. By using a simple co-precipitation method pure (ZnO) (x = 0) and Mg-doped ($Zn_{1-x}MgxO$) (x = 1%, 3% & 5%) nanoparticles were synthesized at 300 ⁰ C. Zinc Nitrate hexa-hydrate, Magnesium acetate, Sodium hydro oxide (NaOH) and demineralized water were used as precursors which are of analytical grade. All the glassware (i.e. long neck round bottom flask, measurement cylinder and beaker) was washed with de-mineralized water and then acetone and then allowed to dry. On an electronic balance, the magnesium acetate, zinc nitrate, and sodium hydroxide is weighed and poured into a round bottom flask as shown. The chemical solution was prepared in a round bottom flask using stochiometric quantities based on the concentration mentioned above. In order to dissolve the chemicals in NaOH a constant stirring was given for 30 minutes at room temperature. Following that, the mixture was held at a steady temperature of 60 ^{o}C at atmospheric pressure until precipitates formed. This procedure took about 5 hours to complete. The solution was then allowed to cool to room temperature while being constantly stirred. The precipitates were allowed to settle for the night before being collected from the solvent. The excess solvent was separated from the precipitates further by centrifuging it at 6000 rpm for 3 minutes on a Select-spin spectra 6c centrifuge machine. The resulting precipitates were dried in an incubator at 80 ^{o}C for around 24 hours to remove the moisture content. He as prepared samples then annealed at 300 ^{o}C for 05 hours in furnace.

2.3. Structural characterization

2.3.1. X-Ray Diffraction

XRD measurements were performed using a *JDX-3532 Jeol, Japan* diffractometer at 35 kV with X-Rays of wavelength (λ = 1.54 ^{o}A). The X-Ray diffractometer was set to operate in steps of 0.02 degree per second. In each step the XRD spectrum of both pure and Mg doped ZnO was observed over a 30^{o} to 70^{o} range. The XRD pattern of pure ZnO samples in figure. 1 indicates its distinctive crystalline structure of 7 peaks. Similarly the XRD pattern showing in figure. 1 of Mg-doped zinc oxide sample shows a similar crystalline structure with 7 peaks as observed for pure ZnO sample. The apparent similarity is due to the low concentration (1%, 3%, and 5%) of dopant Mg. However, a close inspection of both XRD patterns shows a slight shift in the peak positions. X-Ray powder diffraction measurements confirmed the phase formation of Zn1-xMgxO, Polycrystalline samples of $Zn_{1-x}Mg_xO$.

The XRD pattern of pure ZnO has prominent peaks at 31.8°, 34.42°, 36.28°, 47.54°, 56.54°, 62.88° and 67.92° whereas the XRD peaks of 1% Mg-doped ZnO sample are at 31.8°, 34.34°, 36.2°, 47.5°, 56.65°, 62.89 and 67.4° and 3% Mg-doped ZnO sample are at 31.53°, 34.18°, 36.05°, 47.34°, 56.39°, 62.64°and 67.79°also 5% Mg-doped ZnO sample are at

31.74°,34.39°,36.23°,47.5°,56.60°,62.840 and 68.0° for Mg doped ZnO sample. It is also confirmed from the XRD spectrum that the synthesized pure and doped ZnO particles are in nanometer range. The average size of nanoparticles is observed to be 36 nm for pure ZnO and 29.25nm, 24.57 and 23.87 nm respectively for Mg-doped ZnO respectively using Debye-Scherrer equation. The observed peaks position and d-value with comparison of standard d-values of ZnO nanoparticles are given in table.1. In this case the small change in d-values is observed but the Miller indices (*hkl*) indicate that the hexagonal structure is obtained. For Mg-doped ZnO, the observed peaks position and d-value with comparison of pure ZnO nanoparticles are given in table3.2 and the small change in d-values is also observed but the Miller indices (*hkl*) indicate that the same hexagonal structure is obtained. XRD analysis revealed that our Zinc Oxide nanoparticles have hexagonal wurtzite structure and all the diffraction peaks were found to be in agreement with JCPDS data. No impurity peaks were observed within the detection limit of XRD.

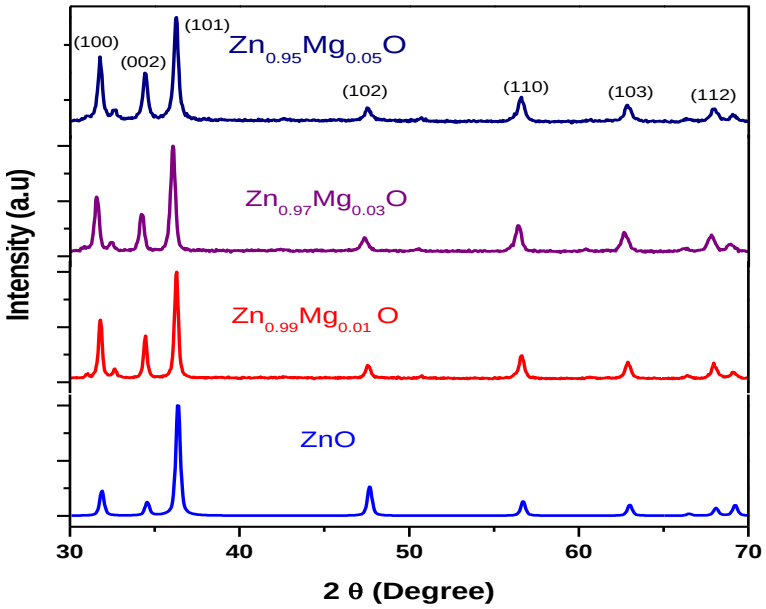

Fig. 1. XRD pattern of pure and (1%, 3% and 5%) Mg-doped ZnO nanoparticles. ZnO estimated parameters from positions of different peaks in the XRD patterns of pure ZnO nanoparticles.

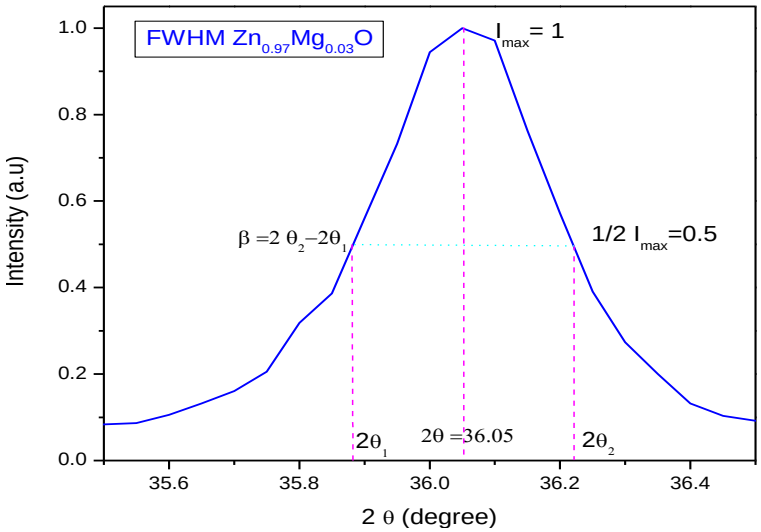

Fig. 2. Full Width Half Maximum of Mg-doped Zinc oxide.

2.3.2. XRD Patterns and Estimation of particle size

By using *Debye-Scherrer* formula, we can calculate the crystallite size of nanoparticles.

$$D = \frac{0.9\lambda}{\beta\cos\theta}$$

where, D = diameter of nanoparticles, λ = Wavelength of X-ray, β = Full width half maxima of peak and θ = Angle obtained from maximum peak intensity in XRD pattern.

Estimation of particle size using *Debye-Scherrer formula*

For example, we calculate particle size of **ZnO**

$$D = \frac{0.9\lambda}{\beta\cos\theta}$$

$$D = \frac{0.9 \times 1.54}{0.49 \times 0.0174 \times \cos(18.02)}$$

$$D = 36 \text{ nm}$$

we calculate particle size of $\mathbf{Zn_{0.99}Mg_{0.01}O}$

$$D = \frac{0.9\lambda}{\beta\cos\theta}$$

$$D = \frac{0.9 \times 1.54}{0.28 \times 0.0174 \times \cos(18.01)}$$

$$D = 29.84 \text{ nm}$$

we calculate particle size of $\mathbf{Zn_{0.97}Mg_{0.03}O}$

$$D = \frac{0.9\lambda}{\beta\cos\theta}$$

$$D = \frac{0.9 \times 1.54}{0.34 \times 0.0174 \times \cos(18.025)}$$

$$D = 24.56 \text{ nm}$$

we calculate particle size of $\mathbf{Zn_{0.97}Mg_{0.03}O}$

$$D = \frac{0.9\lambda}{\beta\cos\theta}$$

$$D = \frac{0.9 \times 1.54}{0.35 \times 0.0174 \times \cos(18.12)}$$

$$D = 23.87 \text{ nm}$$

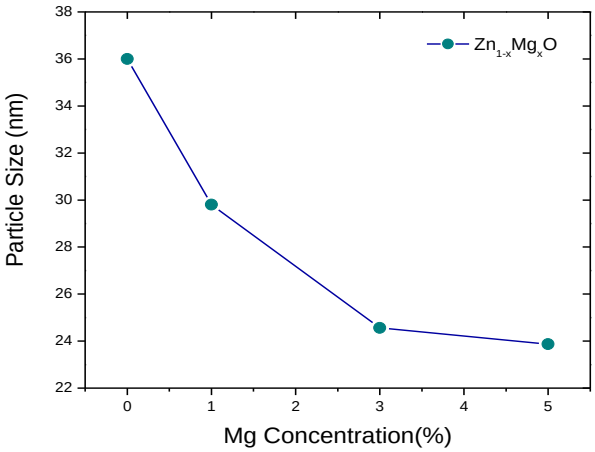

Fig. 3 Particle size verses Mg concentration

.

Table 1. Peaks position of pure and Mg doped ZnO nanoparticles.

Peaks	**Miller indices (h, k, l)**	**2θ for Pure ZnO**	**2θ for $Zn_{0.99}Mg_{0.01}O$**	**2θ for $Zn_{0.97}Mg_{0.03}O$**	**2θ for $Zn_{0.95}Mg_{0.05}O$**
1st Peak	(100)	31.8	31.8	31.53	31.74
2nd Peak	(002)	34.42	34.34	34.18	34.39
3rd Peak	(101)	36.28	36.2	36.05	36.237
4th Peak	(102)	47.54	47.5	47.34	47.75
5th Peak	(110)	56.54	56.65	56.39	56.60
6th Peak	(103)	62.88	62.897	62.64	62.84
7th Peak	(112)	68.92	67.90	67.79	68.0

Table 2. d-value parameter of pure and Mg doped ZnO nanoparticles.

Peaks	Miller indices (h, k, l)	Observed Value Pure ZnO	Observed Value $Zn_{0.99}Mg_{0.01}O$	Observed Value $Zn_{0.97}Mg_{0.03}O$	Observed Value $Zn_{0.95}Mg_{0.05}O$
1st Peak	(100)	2.81	2.81	2.835	2.82
2nd Peak	(002)	2.60	2.61	2.62	2.60
3rd Peak	(101)	2.47	2.478	2.49	2.47
4th Peak	(102)	1.91	1.91	1.92	1.91
5th Peak	(110)	1.62	1.62	1.63	1.625
6th Peak	(103)	1.47	1.476	1.48	1.48
7th Peak	(112)	1.37	1.38	1.38	1.377

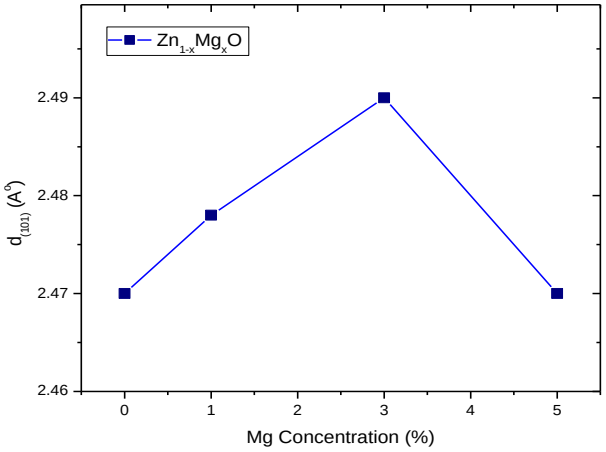

Fig. 4 d-value verses Mg concentration.

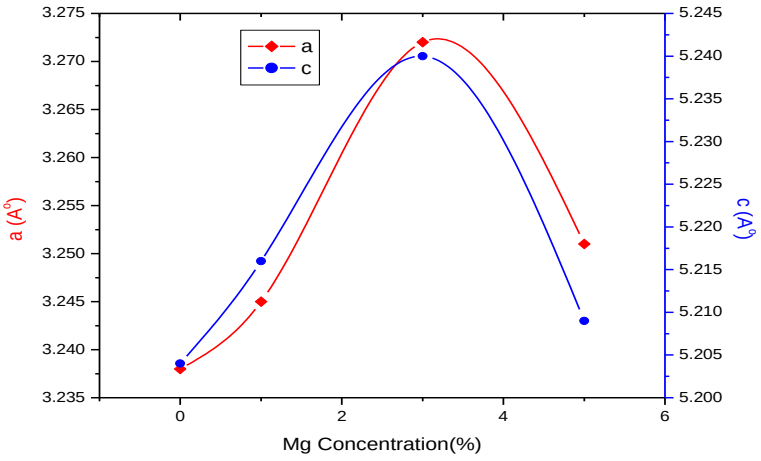

Fig. 5. Lattice parameter vs Mg concentration.

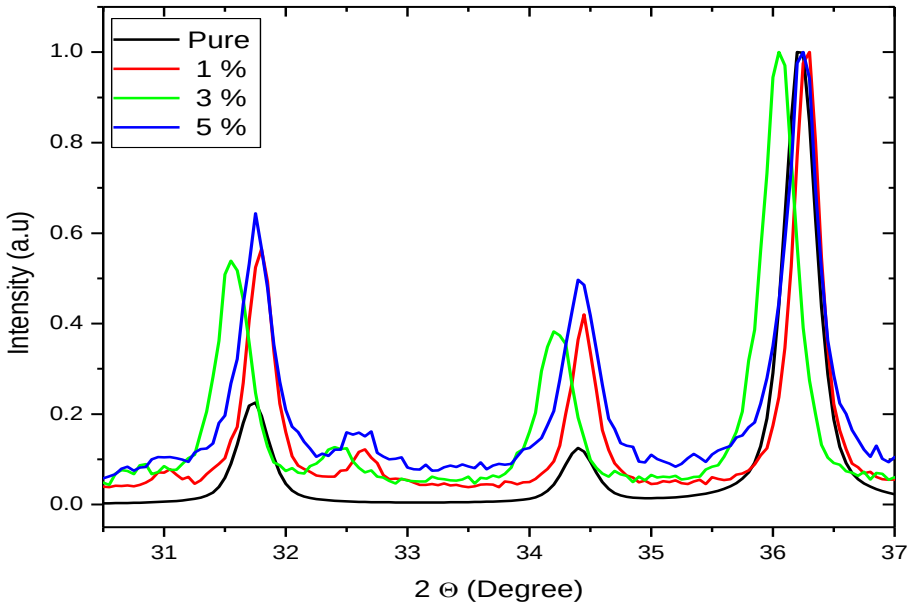

Fig. 6. XRD pattern of peaks (100),(002),(101) pure and (1%, 3% & 5%) Mg-doped ZnO nanoparticles. θ

Particle size reduced by increasing of doping due to Mg^{+2}(0.57A^o) replace Zn^{+2} (0.60A^o) No other impurities was found in this pattern, which exhibit hexagonal phase structure. In XRD patterns of Mg doped ZnO nanoparticle show peaks near 32.6^o which is attributed to MgO secondary phase. This diffraction peaks is assigned to the diffraction from (311) MgO plane. It was found that pure ZnO has a crystalline size of 36 nm, but as the Mg concentration increases, it shrinks to 23 nm. (See Fig. 3).

2.4. Scanning electron microscopy studies (SEM)

SEM images depict the surface morphologies of pure ZnO and Mg-doped ZnO (1%, 3% and 5%) nanostructures. It could be observe that pure ZnO and 1% Mg doped ZnO have rod like structure.

The morphology changes to spherical for samples having 3% Mg doping. Interestingly upon increasing Mg concentration up to 5% the Nanospheres transforms into Nanosheets. The observed morphological transformation in our samples is consistent with the literature. The ZnO nanostraucture can be defined as a series of alternating planes made up of tetrahedral coordinated Zn^{+2} and O^{-2} ions. The positively charged $(000\bar{1})$ Zn polar surfaces and negatively charged $(000\bar{1})$ O polar surfaces generated by the oppositely charged ions results in a regular dipole along the c-axis.

One expects morphology of nanoparticles to represent a minimum of surface energy. Therefore, in many cases, nanoparticles are spherical in shape, at least facetted particles, which are close to a sphere. To understand the reason for non-spherical nanoparticles, one has to look at the crystalline structure and to the method of synthesis. The surface energy of different crystallographic planes depends on their orientations. For example, in cubic structure, the planes describing a cube have the lowest surface energy. The discussion is most important in non-cubic systems. Depending on the surface energy of the different planes, non-cubic substances may have a tendency to crystallize in rods or plates [11]. The surface energy is modified by surface-active substances, also in the case of cubic structures, rods or plates are obtainable.

The dependency of the surface energy on the crystallographic plane has consequences on the shape of nanoparticles: assuming a prism with a quadratic base with an edge length **a**, and a height **c** one obtains a rod-like prism in the case that the surface energy of the base plane is large compared to that of the side plane. In the other case, one obtains a plate-like prism. The ratio of the sides of a tetragonal prism is equal to the ratio of the surface energies. This is the rule for the formation of nanorods or nanoplates that can be derive from thermodynamics

Surface energy is the reason for non-spherical nanostructures in case of anisotropic (non-cubic) crystal structures. As assuming, a tetragonal bodies with the sides *a*, *c* and the specific surface energies γ_a and γ_c. SEM analysis indicates that as Mg concentrations increase, our samples' morphology shifts from rod-like to sheet-like structures. We infer that the morphology transformation is caused by impurities of Mg in ZnO since the synthesis process for all samples is nominally identical except for the initial concentration of Mg precursor. Positively Zn^{+2} terminated (0001) and negatively O^{-2} terminated $(000\bar{1})$ polar planes are constituted in the hexagonal unit cell of ZnO, resulting in a net dipole moment along c axis, which explicates the morphological evolution in the samples. Also there exists nonpolar faces, like $(01\bar{1}0)$ planes. The surface energies of polar (0001) planes have been found to be greater than nonpolar $(01\bar{1}0)$ planes. It causes energetically favorable growth along the c-axis. The existence of large amount of OH^{-1} ions in the solution is another factor that regulates the growth mechanism. The growth of Zn^{+2} terminated (0001) planes is supported by these OH^{-1} ions. This precedes the rod-like morphology of the sample. This is consistent with previous studies which found that the interaction of OH^{-1} ions promotes the formation of elongated rod-like structures. In the limit of low doping (x≤1%) concentrations, the 1D growth mode dominates for pure ZnO and Mg doped ZnO nanostructures. Above x>1%, the proportion of OH^{-1}decreases due to the higher acidity of the Mg $(CH_3COO)_2$ solution. In this case, to minimize electrostatic repulsion, excess Mg^{+2} ions can preferentially diffuse to low energy non-polar plane, i.e., $(0\bar{1}00)$, $(\bar{1}010)$, $(1\bar{1}00)$, $(01\bar{1}0)$, $(10\bar{1}0)$. As a result, the sample's morphology changes to flower-like (along non-polar planes) from rod-like (along

polar planes). The observation that growth velocities on non-polar planes are considerably greater than those on polar planes supports 2D growth in these directions. Scanning electron microscopy (SEM) images are shown in Fig.9. The cylindrical rod -like, sphere-like and sheets-like morphology is clearly visible.

Fig. 7. Scanning Electron Microscope (SEM) images of pure ZnO rod like nanoparticles.

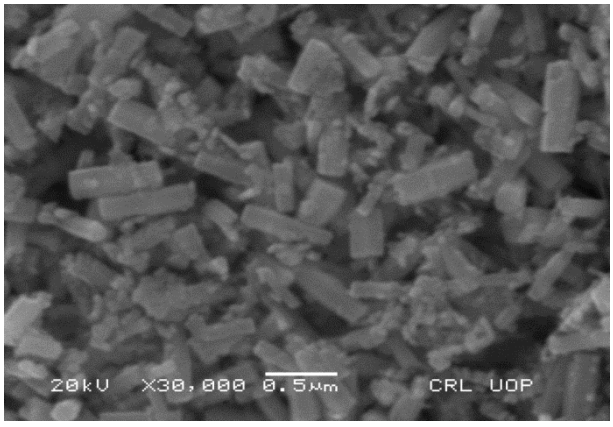

Fig. 8. Scanning Electron Microscope (SEM) images of $Zn_{0.99}Mg_{0.01}O$ rod like nanoparticles.

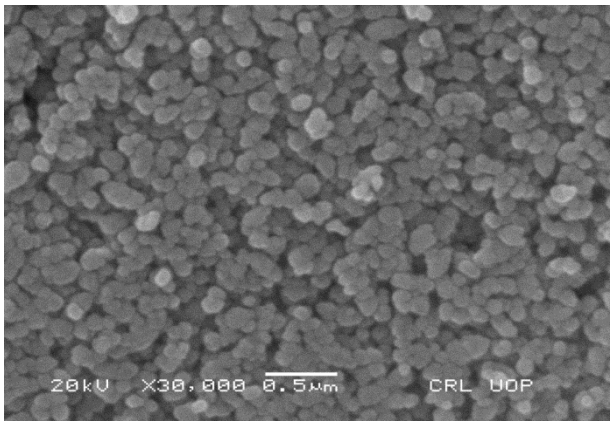

Fig. 9. Scanning Electron Microscope (SEM) images of $Zn_{0.97}Mg_{0.03}O$ sphere like nanoparticles.

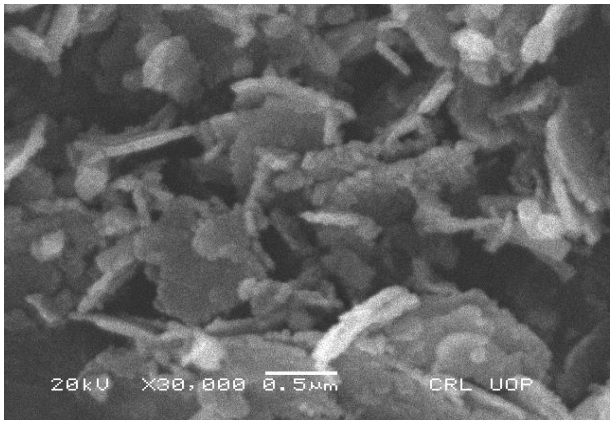

Fig. 10. Scanning Electron Microscope (SEM) images of $Zn_{0.95}Mg_{0.05}O$.

2.5. Energy Dispersive spectroscopy (EDS) of pure an Mg doped ZnO nanoparticles

The results of the EDX study show that there are no impurities in the pure and Mg doped ZnO nanoparticles, and that Mg doping has no effect on the wurtzite structure of ZnO due to its small quantity and nearly identical radius sizes.

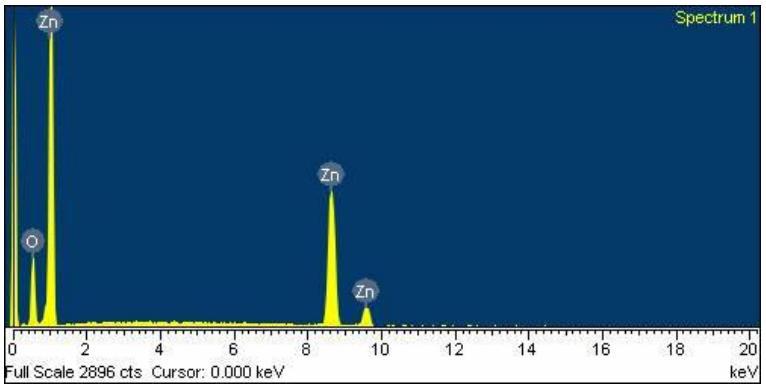

Fig. 11. EDX spectrum of the Pure ZnO nanoparticles.

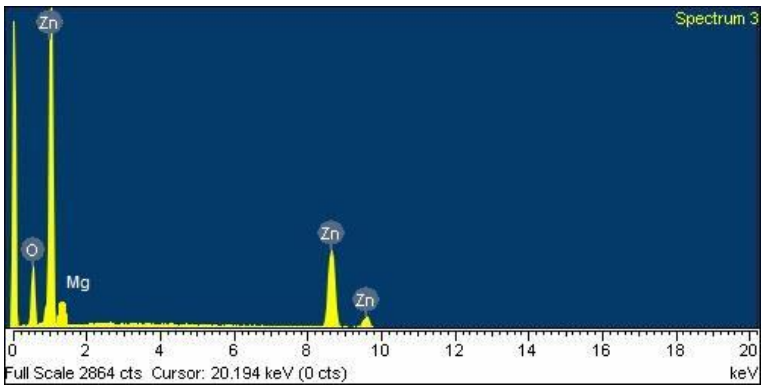

Fig. 12. EDX spectrum of the Mg doped ZnO nanoparticles.

2.6. UV- Visible spectroscopy

The UV-Vis absorption spectra of pure and Mg doped ZnO nanoparticles shown in Figure 13 indicates the clear shift towards the shorter wavelength. The absorption to short wavelength

causes increase band gap. The optical band gap energies evaluated from the obtained absorption spectra are increasing from 3.37 to 3.74 eV for $Zn_{1-x}Mg_xO$ (x = 0 to 0.05), respectively.

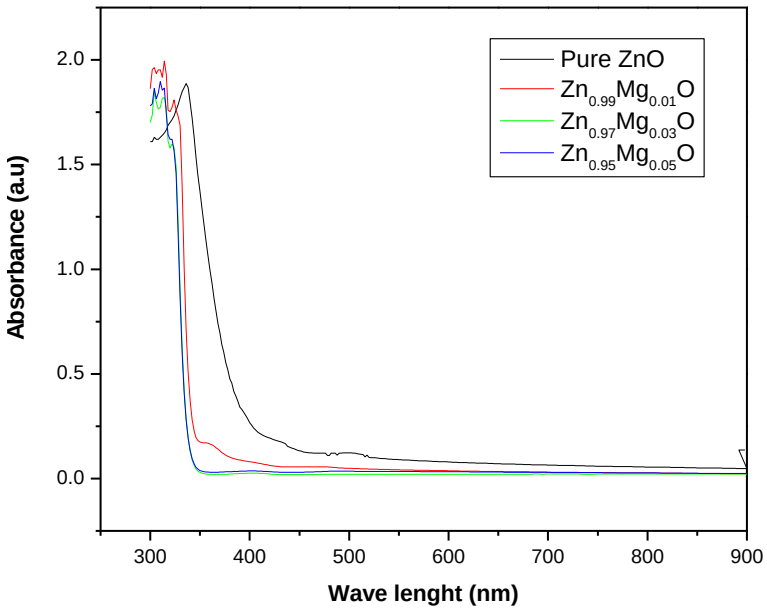

Fig. 13. The UV-VIS spectra for pure and (1%, 3% and 5%) Mg-doped ZnO samples distinct peaks achieved in the UV region near 335 nm, 311 nm, 310.6 nm & 310 nm respectively showings towards blue shift.

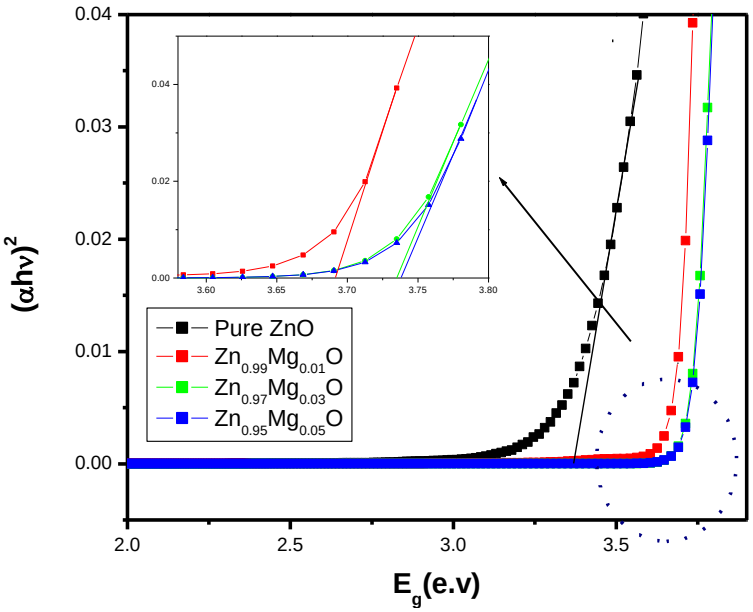

Fig. 14. $(\alpha h\upsilon)^2$ vs. photon energy ($h\upsilon$) of $Zn_{1-x}Mg_xO$ nanoparticles for determination of band gap (E_g).

Most important factor in semiconductor physics is band gap energy. Which explains the opto-electronic applications. The band gap of nanoparticles can be altered with the size of the particle. The wide band gap related with high excitonic binding energy made it member in LASERs and LEDs in ultra violet region. In opto-electronic device applications of ZnO nanotubes and nanorods it uses for optical properties controlling by adjusting the performance of device

The energy band gap calculation of pure and (1%, 3% and 5%) Mg-doped samples using Tauc-plot method, band gap found 3.37 e.V, 3.69 e.V, 3.73 e.V & 3.74e.V. The band gap of pure

ZnO is 3.37 eV, indicating a blue shift. Moreover, for Mg-doped ZnO samples the band gap has been increased remarkably and found to be 3.74 e.V.

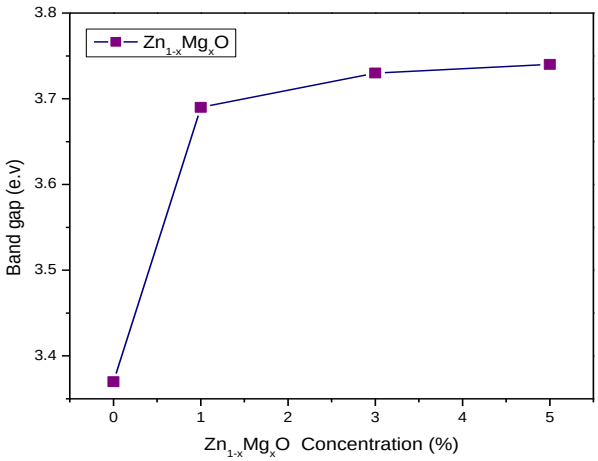

Fig. 15. Band gap vs Mg concentration.

3. Conclusion

We conducted systematic studies on both the structural and optical properties of pure and Mg doped ZnO nanoparticles in our present work. Using our experimental observations we have come up with the following conclusions.

Pure and Mg doped nanoparticles were successfully synthesized using a simple and low cost chemical route *i.e.* by adopting a modified co-precipitation method. The structural characterization of the prepared sample was done by XRD and SEM analysis. The results obtained from these techniques confirmed the formation of pure and Mg doped ZnO nanoparticles. Significant agglomeration of nanoparticles was noticed in both pure and Mg doped nanoparticles by SEM images.

It is found that the prepared samples of all pure and Mg-doped ZnO have Wurtzite hexagonal structure. The average size of the nanoparticles of pure and (1%, 3% and 5%) Mg doped ZnO calculated from Debye-Scherrer formula is found to be 36 nm, 29nm, 24.57 and 23.87 nm respectively. However, it is observed that the particle size found from SEM analysis is larger than the size obtained from XRD analysis. The nanoparticles have a crystalline structure and morphology similar to rods, spheres and sheets, as shown by SEM images of synthesized samples.

The EDX analysis results confirms that the compositions of the pure and Mg doped ZnO nanoparticles having no impurities, and Mg doping has not affected on the wurtzite structure of ZnO because of its small quantity and almost similar radius sizes. The UV peaks present in the spectra of both pure and (1%, 3% and 5%) Mg doped ZnO samples are attributed to the free exciton transition which is an intrinsic feature of the wurtzite ZnO and has its origin in the excitonic recombination. Radiative transitions of electrons captured at oxygen vacant sites with holes trapped at singly ionized oxygen vacancies are responsible for the broad absorbance peak in the visible region of UV-Visible spectra of Mg doped ZnO sample. The UV-Visible spectra of pure and (1%, 3% and 5%) Mg doped ZnO samples show distinct peaks in the UV region around 335 nm, 311 nm, 310.6 nm and 310 nm, respectively, indicating a blue shift.

Finally, we have calculated the energy band gap of pure and (1%, 3% and 5%) Mg-doped samples using Tauc plot, band gap found 3.37 e.V, 3.69 e.V, 3.73 e.V & 3.74 e.V pure and (1%, 3% and 5%) Mg doped ZnO respectively. The band gap of pure ZnO sample is found to be 3.37 eV which indicates a blue shift in the band gap of ZnO nanopaticles from its bulk gap 3.37 eV. Moreover, for Mg doped samples the band gap has been increased remarkably and found to be 3.74 eV.

References

[1] Ali, A., A.-R. Phull, and M. Zia, Nanotechnology Reviews, 2018. 7(5): p. 413-441; https://doi.org/10.1515/ntrev-2018-0067

[2] Zolfaghari, M. and M. Chireh, Advanced Materials Research. 2014. Trans Tech Publ.; https://doi.org/10.4028/www.scientific.net/AMR.829.784

[3] Li, H., et al., Chemistry of Materials, 2012. 24(15): p. 3044-3055; https://doi.org/10.1021/cm301596x

[4] Kabir, N., et al., RSC Advances, 2014. 4(18): p. 9012-9020; https://doi.org/10.1039/C3RA46093B

[5] Król, A., et al., Advances in colloid and interface science, 2017. 249: p. 37-52; https://doi.org/10.1016/j.cis.2017.07.033

[6] Manna, A.C., Nano-Antimicrobials. 2012, Springer. p. 151-180; https://doi.org/10.1007/978-3-642-24428-5_5

[7] Zak, A.K., et al., International journal of nanomedicine, 2011. 6: p. 1399; https://doi.org/10.2147/IJN.S19693

[8] Joshi, S. and S. Leela, Materials Today: Proceedings, 2021. 43: p. 3166-3168; https://doi.org/10.1016/j.matpr.2021.01.658

[9] Jagadish, C. and S.J. Pearton, Zinc oxide bulk, thin films and nanostructures: processing, properties, and applications. 2011: Elsevier.

[10] Zada, A., et al., Zeitschrift für Physikalische Chemie, 2022. 236(1): p. 53-66; https://doi.org/10.1515/zpch-2020-1778

[11] Espitia, P.J.P., et al., Food and bioprocess technology, 2012. 5(5): p. 1447-1464; https://doi.org/10.1007/s11947-012-0797-6

[12] Wang, L., et al., The Journal of Physical Chemistry C, 2012. 116(3): p. 2074-2079; https://doi.org/10.1021/jp205092e

[13] Alothman, A.A. and M.D. Albaqami, Applied Organometallic Chemistry, 2020. 34(10): p. e5827; https://doi.org/10.1002/aoc.5827

[14] Klaa, K., et al., Phase Transitions, 2020. 93(7): p. 654-665; https://doi.org/10.1080/01411594.2020.1771562

[15] Lim, T., et al., CrystEngComm, 2018. 20(38): p. 5688-5694; https://doi.org/10.1039/C8CE00799C

[16] Qi, J., et al., Materials Chemistry and Physics, 2018. 211: p. 168-171; https://doi.org/10.1016/j.matchemphys.2018.02.016

[17] Aravind, A. and M. Jayaraj, Nanostructured Metal Oxides and Devices. 2020, Springer, Singapore. p. 233-269; https://doi.org/10.1007/978-981-15-3314-3_8

[18] Nguyen, T., et al., Results in Materials, 2020. 6: p. 100088; https://doi.org/10.1016/j.rinma.2020.100088

[19] Ohring, M., Materials science of thin films. 2001: Elsevier. https://doi.org/10.1016/B978-012524975-1/50004-5

[20] Pandey, A., et al., Structural characterization of polycrystalline thin films by X-ray diffraction techniques. Journal of Materials Science: Materials in Electronics, 2021: p. 1-28.

[21] Tiwari, N., et al., RSC advances, 2017. 7(89): p. 56662-56675; https://doi.org/10.1039/C7RA10748J

[22] Zhang, J.Z., Optical properties and spectroscopy of nanomaterials. 2009: World Scientific; https://doi.org/10.1142/7093

[23] Rösch, F., 1. The atom's structure I: Electrons and shells, in Introduction. 2014, De Gruyter. p. 1-36; https://doi.org/10.1515/9783110221923.1

[24] Ullah, N., et al., International Journal of Environmental Analytical Chemistry, 2016. 96(11):

p. 1048-1058; https://doi.org/10.1080/03067319.2016.1232720
[25] Özgür, Ü. and H. Morkoç, Thin Films and Nanostructures. 2006, Elsevier. p. 175-239; https://doi.org/10.1016/B978-008044722-3/50005-1
[26] Bomila, R., S. Suresh, and S. Srinivasan, Journal of Materials Science: Materials in Electronics, 2019. 30(1): p. 582-592; https://doi.org/10.1007/s10854-018-0324-2
[27] Aspoukeh, P.K., A.A. Barzinjy, and S.M. Hamad, International Nano Letters, 2021: p. 1-16; https://doi.org/10.1007/s40089-021-00349-7
[28] David, S.P., et al., Metal and Metal Oxides for Energy and Electronics. 2021, Springer. p. 185-250; https://doi.org/10.1007/978-3-030-53065-5_6
[29] Teke, A., et al., Physical Review B, 2004. 70(19): p. 195207; https://doi.org/10.1103/PhysRevB.70.195207
[30] Kumbhakar, P., et al., Chalcogenide letters, 2008. 5(12): p. 387-394.
[31] Marques, A.C., R.E. Rojas-Hernandez, and R.M. Journal of Sol-Gel Science and Technology, 2021. 100(1): p. 1-43; https://doi.org/10.1007/s10971-021-05592-0
[32] Borysiewicz, M.A., Crystals, 2019. 9(10): p. 505; https://doi.org/10.3390/cryst9100505
[33] Hussain, S., Investigation of structural and optical properties of nanocrystalline ZnO. 2008, Institutionen för fysik, kemi och biologi.
[34] Neamen, D.A., Semiconductor physics and devices: basic principles. 2003: McGraw-hill.
[35] Peter, Y. and M. Cardona, Fundamentals of semiconductors: physics and materials properties. 2010: Springer Science & Business Media.
[36] Fang, X., et al., Critical Reviews in Solid State and Materials Sciences, 2009. 34(3-4): p. 190-223; https://doi.org/10.1080/10408430903245393
[37] Singh, S., Journal of Nanoengineering and Nanomanufacturing, 2013. 3(4): p. 283-310; https://doi.org/10.1166/jnan.2013.1147
[38] Zou, Y., et al., Sensors, 2018. 18(7): p. 2072; https://doi.org/10.3390/s18072072
[39] Ellmer, K. and A. Bikowski, Journal of Physics D: Applied Physics, 2016. 49(41): p. 413002; https://doi.org/10.1088/0022-3727/49/41/413002
[40] Avrutin, V., D.J. Silversmith, and H. Morkoç, Proceedings of the IEEE, 2010. 98(7): p. 1269-1280; https://doi.org/10.1109/JPROC.2010.2043330
[41] Hou, Q., M. Qi, and Y. Li, Physica Scripta, 2021. 96(12): p. 125815; https://doi.org/10.1088/1402-4896/ac2380
[42] Galdámez-Martinez, A., et al., Nanomaterials, 2020. 10(5): p. 857; https://doi.org/10.3390/nano10050857
[43] Nandi, A., et al., Journal of Materials Science: Materials in Electronics, 2017. 28(15): p. 10885-10892; https://doi.org/10.1007/s10854-017-6867-9
[44] Chen, L., et al., Applied Surface Science, 2019. 467: p. 22-29; https://doi.org/10.1016/j.apsusc.2018.10.132